Title

Structural Evolution and Atom Clustering in beta-SiAlON: beta-$Si_{6-z}Al_zO_zN_{8-z}$

Journal

Inorganic Chemistry, 56(4)

ISSN

0020-1669 1520-510X

Authors

Cozzan, Clayton
Griffith, Kent J
Laurita, Geneva
et al.

Publication Date

2017-02-06

DOI

10.1021/acs.inorgchem.6b02780

Peer reviewed

Structural evolution and atom clustering in β-SiAlON: β-$Si_{6-z}Al_zO_zN_{8-z}$

Clayton Cozzan,[†,‡,¶] Kent J. Griffith,[§] Geneva Laurita,[†,¶] Jerry G. Hu,[¶] Clare P. Grey,[*,§] and Ram Seshadri[*,†,‡,¶,‖]

†*Mitsubishi Chemical Center for Advanced Materials, University of California Santa Barbara, California 93106, United States*

‡*Materials Department, University of California Santa Barbara, California 93106, United States*

¶*Materials Research Laboratory, University of California Santa Barbara, California 93106, United States*

§*Department of Chemistry, University of Cambridge Lensfield Road, Cambridge CB2 1EW, United Kingdom*

‖*Department of Chemistry and Biochemistry, University of California Santa Barbara, California 93106, United States*

E-mail: cpg27@cam.ac.uk; seshadri@mrl.ucsb.edu

Abstract

SiAlON ceramics, solid solutions based on the Si_3N_4 structure, are important, lightweight structural materials with intrinsically high strength, high hardness, and high thermal and chemical stability. Described by the chemical formula β-$Si_{6-z}Al_zO_zN_{8-z}$, from a compositional viewpoint, these materials can be regarded as solid solutions between Si_3N_4 and Al_3O_3N. A key aspect of the structural evolution with increasing Al and O (z in the formula) is to understand how these elements are distributed on the β-Si_3N_4 framework. The average and local structure evolution of highly phase-pure samples of β-$Si_{6-z}Al_zO_zN_{8-z}$ with z = 0.050, 0.075, and 0.125 are studied here, using a combination of X-ray diffraction, nuclear magnetic resonance studies, and density functional theory calculations. Synchrotron X-ray diffraction establish sample purity and indicate subtle changes in average structure with increasing Al content in these compounds. ^{27}Al solid-state magic angle spinning nuclear magnetic resonance (NMR) experiments, coupled with detailed *ab initio* calculations of NMR spectra of Al in different AlO_qN_{4-q} tetrahedra ($0 \leq q \leq 4$), reveal a tendency of Al and O to cluster in these materials. Independently, the calculations suggest an energetic preference for Al–O bond formation, instead of a random distribution, in the β-SiAlON system.

Introduction

SiAlON ceramics can be regarded as solid solutions between the compositions Si_3N_4 and Al_3O_3N. These ceramics are useful for their excellent mechanical properties, such as high hardness, high strength, wear resistance, and resistance to thermal shock.[1] In these systems, Al is substituted for Si, and concomitantly, O for N. In SiAlONs, anion ordering is driven by differences in bonding, size, and charge, and the resultant clustering can have large effects on the behavior of optical SiAlONs.[2] To understand anion ordering in SiAlONs, local structure techniques must be utilized. X-ray diffraction is not sufficient, as the scattering factors of both Si and Al, and O and N are too similar, preventing precise occupancy information from being obtained. Extended X-ray absorption fine structure (EXAFS) suffers the same issues of contrast and is difficult to implement when substituent concentrations are low. The neutron pair distribution function technique could cast light on the problem, but once again, this technique would be limited in utility and scope at the low concentrations of Al and O considered here. Solid-state magic angle spinning nuclear magnetic resonance (MAS NMR) of ^{27}Al offers a potential solution, providing insight into the local coordination environment of the aluminum nucleus.

Early structural investigation of $Si_{6-z}Al_zO_zN_{8-z}$ using MAS NMR observed that ^{27}Al is a sensitive nucleus to coordination and geometry, whereas ^{29}Si is not, with spectra showing Si tetrahedrally coordinated in SiAlON that does not change with increased Al and O substitution.[3,4] Investigations of SiAlONs using ^{27}Al MAS NMR revealed that rather than a random distribution of Si and Al on metal sites and O and N on non-metal sites or a preference for Al-N and Si-O bonds, there is a preference for Al–O and Si–N bonds.[4–6] This preference has also been verified using Monte Carlo simulations and neutron diffraction on other SiAlON systems.[7] Most early NMR studies suggested the existence of mixed tetrahedra,[8] which was supported by EXAFS showing a decrease of the average bond length for the first coordination sphere of Si with increasing Al and O.[4]

Broadening is observed in ^{27}Al MAS NMR spectra, and is associated with distorted tetra-

hedra from a range of AlO_qN_{4-q} ($0 \leq q \leq 4$). It was proposed that the distribution changes with decreasing Al as more of the mixed AlO_3N and AlO_2N_2 are present, which are broader, and the AlN_4 peak intensity decreases with increasing Al due to AlO_3N and AlO_2N_2 formation.[6] As the composition of SiAlON approaches AlN, the proportion of AlN_4 tetrahedra increases relative to $AlON_3$ tetrahedra.[8,9] Conversely, in the formula $Si_{3-z}Al_zO_zN_{4-z}$ for z $\approx$ 0.5 to 1, it was observed that substitutional O is strictly coupled to $Al(O,N)_4$ tetrahedra with a range of tetrahedral coordinations.[5] These early NMR works observed changes in lineshape as a function of Al–O content, but could not resolve them into distinct coordination environments due to the moderate fields used. More recently, work using X-ray absorption near edge spectroscopy (XANES) and computation showed evidence for Al–O bonds in SiAlON, with pairing of Al and O having an energy benefit of a few tenths of an eV per Al–O pair.[10]

Here, samples of β-$Si_{6-z}Al_zO_zN_{8-z}$ with systematically varying Al content ($z = 0.050$, $z = 0.075$, and $z = 0.125$) are studied. Synchrotron X-ray diffraction was utilized to investigate average structure changes in this system as a function of systematic variation in Al content. Synchrotron X-ray diffraction and prior neutron scattering work on the same samples (to establish composition) confirm phase purity, as well as demonstrate that the actual composition is the nominal composition.[11] *Ab initio* periodic density-functional theory (DFT) based calculations of NMR parameters and structural energetics, along with high-field ^{27}Al MAS NMR measurements were employed to elucidate local structure details of the Al site in the SiAlON structure. Improvements in NMR hardware, coupled with quantum calculations, have enabled the identification and quantification of the aluminum coordination environments. Simulations of quadrupolar NMR lineshapes highlight the inherent inability of previous moderate field studies to resolve any but the highly symmetric AlO_4/AlN_4 sites. Clustering of Al and O in the SiAlON structure is observed experimentally and is supported independently by DFT enthalpies and comparison of calculated Al environments to experimental spectra collected in the current work. The current work is

therefore the first high field NMR study of completely phase pure β-$Si_{6-z}Al_zO_zN_{8-z}$, and is also the first time DFT calculations have been employed to to assign spectra and determine energetics in these systems.

Besides helping to understand the distribution of Al and O in β-SiAlON phases, the present work points to the general utility of employing high-resolution, high-field NMR techniques, in appropriate combination with DFT calculations to unravel the intricate details of local compositional variation in functional materials. Studies such as these could profit a variety of functional material classes where small amounts of dopants are known to have important effects. These include zeolites,[12] phosphors,[11,13] diluted magnetic semiconductors,[14] and thermoelectric materials.[15]

Methods

To obtain accurate control over the concentration of Al^{3+} and O^{2-}, a high-pressure and high-temperature synthesis route was used. Powders of α-Si_3N_4 and Al_2O_3 were ground with nominal stoichiometry $Si_{6-z}Al_zO_zN_{8-z}$ in an alumina pestle. The powders were heated in a boron nitride crucible at 1950 °C for 12 h under N_2 (>99.9995%) at a pressure of 0.92 MPa and annealed in argon for 8 h before being ground into a fine powder and washed using a mixture of HNO_3 and HF.

Synchrotron X-ray powder diffraction was performed at room temperature at the 11-BM beamline at the Advanced Photon Source, Argonne National Laboratory. The calibrated wavelength was $\lambda = 0.459001$ Å for $z = 0.075$ and $\lambda = 0.413194$ Å for $z = 0.050$ and $z = 0.125$. Rietveld refinements were performed using the General Structure Analysis System (GSAS) with EXPGUI.[16,17] Peak shapes were handled using the pseudo-Voigt profile function, which combines Gaussian and Lorentzian components. The background was handled using a Chebyshev polynomial. The occupancies were left as nominal due to the lack of contrast of scattering between Al and Si and between O and N. The refined structures

were visualized using the open-source crystallographic software VESTA.[18]

Solid-state ^{27}Al NMR was conducted at room temperature using a Bruker AVANCE III Ultrashield Plus 800 MHz (18.8 T) narrow bore (54 mm) spectrometer with a 3.2 mm Tri-Gamma HXY triple resonance MAS probe with a transmitter frequency of 208.52 MHz for the 100% naturally abundant ^{27}Al nuclei. Samples were packed into a 3.2 mm zirconia rotor (Bruker) and spun at 20 kHz for 24 h of data collection due to low Al content. The radio frequency (RF) pulse length (3.6 μs) and power (117.5 W) were chosen to achieve a 15 degree pulse ($\pi/12$) rotation of the net ^{27}Al magnetization for quantitative measurements. Shifts were referenced to 1 M $Al(NO_3)_{3(aq.)}$ at 0 ppm. The resonance frequency for nuclei with non-zero nuclear quadrupolar coupling constants (NQCC, C_Q) is influenced by electronic shielding as well as a quadrupolar term, thus it is correct to refer to shifts, rather than chemical shifts, for quadrupolar nuclei such as ^{27}Al. Data treatment was performed using the SOLA interface in Topspin 3.2. Simulations were performed on the central ($+1/2 \leftrightarrow -1/2$) and satellite transitions ($\pm 1/2 \leftrightarrow 3/2$ and $\pm 3/2 \leftrightarrow 5/2$) with second-order perturbation theory treatment of the quadrupolar interaction. *Ab initio* DFT calculations of enthalpy and NMR parameters were performed in the CASTEP plane-wave code.[19–22] The Perdew–Burke–Ernzerhof (PBE)[23] exchange-correlation functional, a generalized gradient approximation (GGA) functional, was employed. Core electrons were approximated with Vanderbilt "ultrasoft" pseudopotentials generated "on-the-fly" in CASTEP 8.0. The SiAlON system required a basis set of plane waves with energies up to 600 eV and a Monkhorst–Pack[24] grid corresponding to a Brillouin zone sampling finer than $2\pi \times$ 0.05 Å^{-1}. Convergence with respect to the basis set energy and Brillouin zone sampling was confirmed. Under these conditions, enthalpy, σ_{iso}, and C_Q were converged to within 0.1 eV, 0.1 ppm, and 0.1 MHz, respectively. The reference equation used to convert shielding to shift was determined via linear regression from a series of Al-compounds and is detailed in the Supporting Information. Numerical simulations of the quadrupolar NMR lineshapes were performed from the *ab initio* ^{27}Al NMR tensors in the SIMPSON[25] program

at 18.8 T and 20 kHz MAS to compare with the spectra collected in this study. The effect of unit cell size in the calculations was evaluated by comparing calculations with the lattice parameters fixed at the values determined from synchrotron diffraction for $z = 0.050$, $z = 0.075$, and $z = 0.125$ as well as when the cell was allowed to relax from the initial values for $z = 0.075$.

Results and discussion

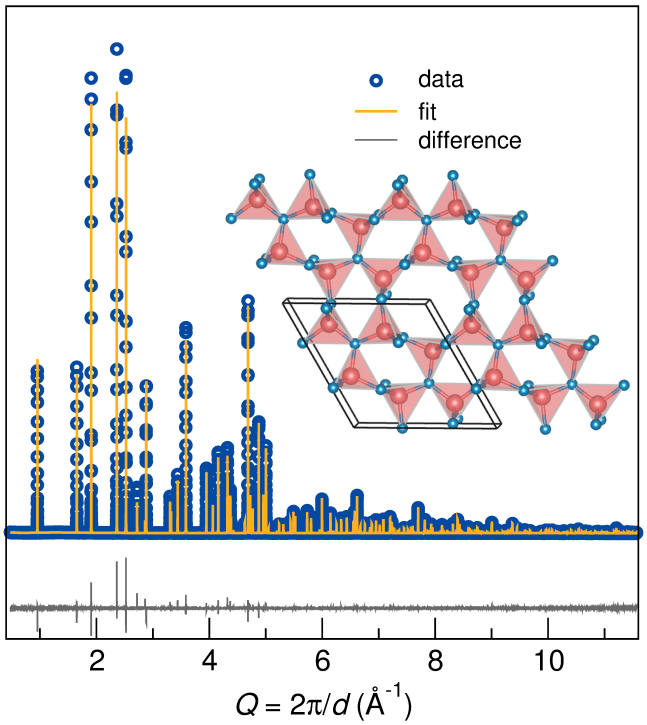

Figure 1: Synchrotron X-ray diffraction data (blue circles), refinement (fit, orange), difference between data and fit (gray line), and refined structure as inset, for β-$Si_{6-z}Al_zO_zN_{8-z}$ with $z = 0.075$.

β-$Si_{6-z}Al_zO_zN_{8-z}$ consists of densely packed, corner sharing (Si,Al)$(O,N)_4$ tetrahedra with ABAB stacking[5] and crystallizes in the hexagonal space group $P6_3$ (no. 173) with a channel along the c-axis.[11,26,27] Rietveld refinements of synchrotron X-ray data indicate phase purity in the β-SiAlON samples. Figure 1 shows the room temperature fit and refined structure for $z = 0.075$, with detailed structural refinements of atomic positions and

Table 1: Structural data obtained from Rietveld refinements of X-ray synchrotron diffraction data for β-$Si_{6-z}Al_zO_zN_{8-z}$ with $z = 0.075$. Numbers in parentheses show standard deviation on the last number. O1 and N1 are located on the 6c Wyckoff site and O2 and N2 are located on the 2b Wyckoff site in the unit cell.

Al content (z)	0.050	0.075	0.125
Cell a (Å)	7.60584(1)	7.60692(2)	7.60853(2)
Cell c (Å)	2.908444(7)	2.909039(7)	2.910116(7)
Cell V (Å^3)	145.7090(4)	145.7800(5)	145.8960(5)
Si/Al x	0.7685(5)	0.7685(4)	0.7685(2)
Si/Al y	0.1747(5)	0.1747(4)	0.1744(2)
Si/Al z	0.291(5)	0.250(3)	0.290(5)
O1/N1 x	0.0298(4)	0.0296(3)	0.0296(4)
O1/N1 y	0.3292(4)	0.3298(3)	0.3296(5)
O1/N1 z	0.303(4)	0.2670(3)	0.6975(4)
O2/N2 z	0.281(7)	0.238(6)	0.28(5)
Si/Al U_{iso} (Å^2)	0.0030(2)	0.0022(5)	0.0035(2)
O1/N1 U_{iso} (Å^2)	0.0031(4)	0.0023(4)	0.0039(6)
O2/N2 U_{iso} (Å^2)	0.0026(9)	0.0006(8)	0.0022(5)

refined atomic displacement parameters (U_{iso}) for all samples shown in Table 1.

Small atomic displacement parameters are linked to high structural rigidity.[11,28] In the present work, the thermal displacement parameters are small, and therefore the rigidity does not change much with small substitution levels. It can be seen that the U_{iso} values for $z = 0.075$ are lowest, but X-ray scattering factors of O and N are too similar, there are not significant differences in any of the U_{iso} values that dictate a clear trend, and differences are in some cases within standard deviation of the refinement. In general, all samples have small atomic displacement parameters, which indicate that the rigidity of the structure is not reduced at small Al substitution levels. Also observed with increasing Al content is the increase in unit cell parameters both in the a and c direction, which leads to an overall increase in the unit cell volume.[5] An ionic radii argument can explain this expansion, as Al^{3+} has a larger radius than Si^{4+} (0.39 Å and 0.26 Å for coordination number CN = 4, respectively).[29] This also involves incorporating O^{2-} to charge balance, which is smaller than N, and therefore would compete with the expansion.

Lattice parameters shown in Table 1 highlight the increase in unit cell volume with

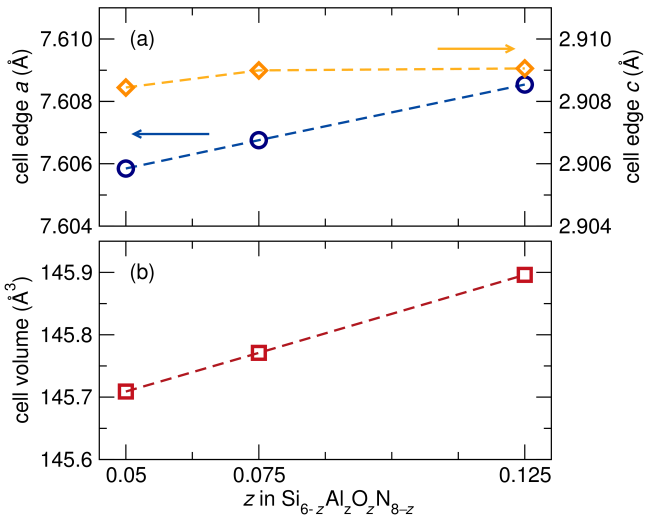

Figure 2: (a) Unit cell edges and (b) volume as a function of z determined through synchrotron X-ray diffraction show an increase in all parameters with z. Error bars are contained within the data points.

increasing Al content (visualized in Figure 2a). While an increase in the unit cell volume does not guarantee an increase in these bond distances, the average bond length around this site increases from 2.6698 Å in $z = 0.050$ to 2.6877 Å in $z = 0.125$.

Si_3N_4 crystallizes in a unit cell with six silicon atoms and eight nitrogen atoms (Z = 2). For *ab initio* calculations, in order to study representative Al and O substitution levels, $2\times2\times2$ (48 Si/64 N, example defect structures shown in Figure 3) and $2\times2\times4$ (96 Si/128 N) supercells were created with Al–O pairs swapped into the new cells, representing $z = 0.0625$ for one Al–O pair in the former supercell, to $z = 1$ for eight Al–O pairs in the later supercell in $Si_{6-z}Al_zO_zN_{8-z}$. For calculations of the defect energetics, unit cell parameters were fixed to the experimental values found in this study for the intermediate Al content ($z = 0.075$) and atomic coordinates relaxed to local minima with DFT forces. Bond lengths obtained from diffraction and DFT show that for Si_3N_4, the Si–N bond lengths range from 1.70 Å to 1.77 Å. In low-Al SiAlONs, the Si–N bond lengths show very slight contraction, with bond lengths ranging from 1.68 Å to 1.76 Å. Si–O (1.74 Å to 1.77 Å), Al–N (1.77 Å to 1.83 Å), and Al–O (1.82 Å to 1.88 Å) bond ranges obtained from DFT confirm that Al forms longer bonds than Si, and O forms longer bonds than N; all

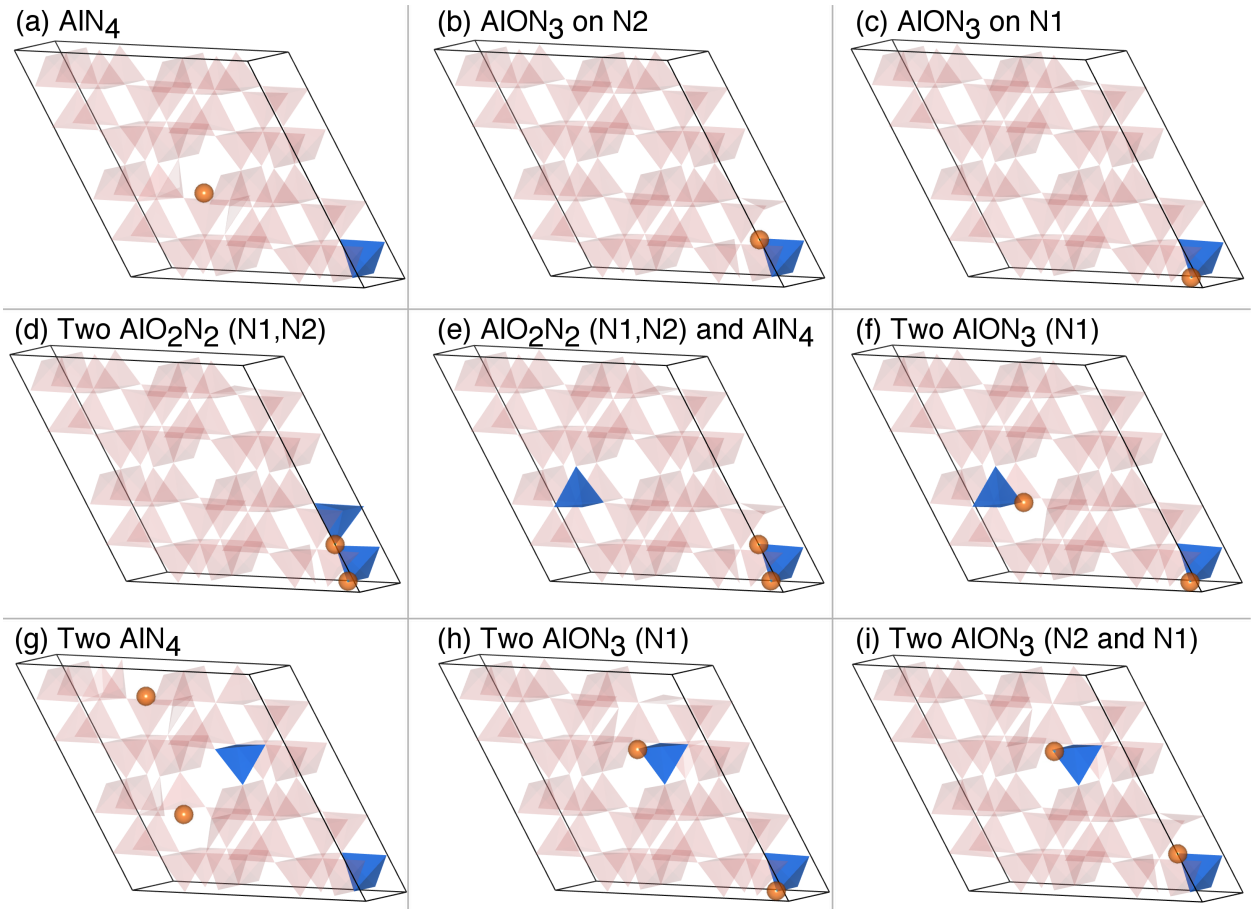

Figure 3: Defect structures for $2 \times 2 \times 2$ supercells with composition $Si_{48-x}Al_xN_{64-x}O_x$, where x=1 for (a)–(c) and x=2 for (d)–(i), are shown. Si–N tetrahedra are red, Al tetrahedra are blue, and oxygen atoms are orange and exaggerated in size for visibility. The defects follow the order of Table 3 and correspond to (a) AlN_4, (b) $AlON_3$ on the N2 site, (c) $AlON_3$ on the N1 site, (d) AlO_2N_2 (N1, N2) and AlO_2N_2 (N1, N2), (e) AlO_2N_2 (N1, N2) and AlN_4, (f) $AlON_3$ (N1) and $AlON_3$ (N1), (g) AlN_4 and AlN_4, (h) $AlON_3$ (N1) and $AlON_3$ (N1), and (i) $AlON_3$ (N2) and $AlON_3$ (N1). The anions O1 and N1 are located on the 6c Wyckoff site and O2 and N2 are located on the 2b Wyckoff site in the supercell.

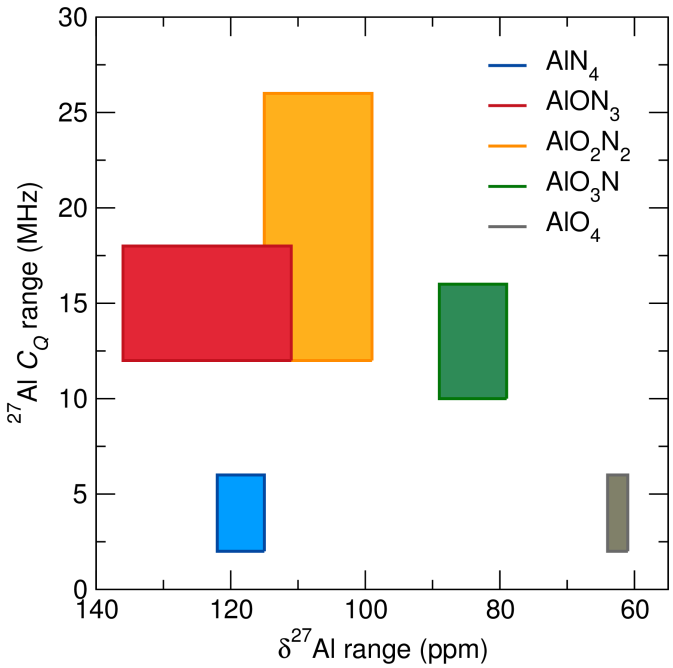

Figure 4: Calculated ranges for ^{27}Al C_Q (MHz) and δ (ppm) for various tetrahedral environments.

of which supports the observation of unit cell expansion with increasing z obtained from Rietveld refinements of the diffraction data.

Table 2: NMR parameters for fits from Figure 5 as informed by DFT calculations. Numbers in parentheses show uncertainties.

Site	AlN_4	$AlON_3$	$AlON_3$	AlO_2N_2/AlO_3N
δ^{27}Al shift (ppm)	108(1)	113(5)	116(5)	96(5)
C_Q (MHz)	3.4(0.5)	11.0(0.5)	12.8(0.5)	13.2(0.5)
η_Q	0.50(0.10)	0.80(0.10)	0.90(0.10)	0.40(0.10)

NMR calculations for magnetic shielding, shielding anisotropy, and the electric field gradient (EFG) tensor were performed. ^{27}Al C_Q ranges (MHz) versus δ (^{27}Al) (ppm) ranges computed in this study are shown in Figure 4. The fits of the experimental NMR data are shown in Figure 5 with parameters shown in Table 2. Lineshapes were fit to the data as informed by the range of values for each parameter from the calculations. Only the central line of the experimental spectra was fit. The relatively low intensity of the spinning sidebands as well as baseline distortions, both common issues for small quanti-

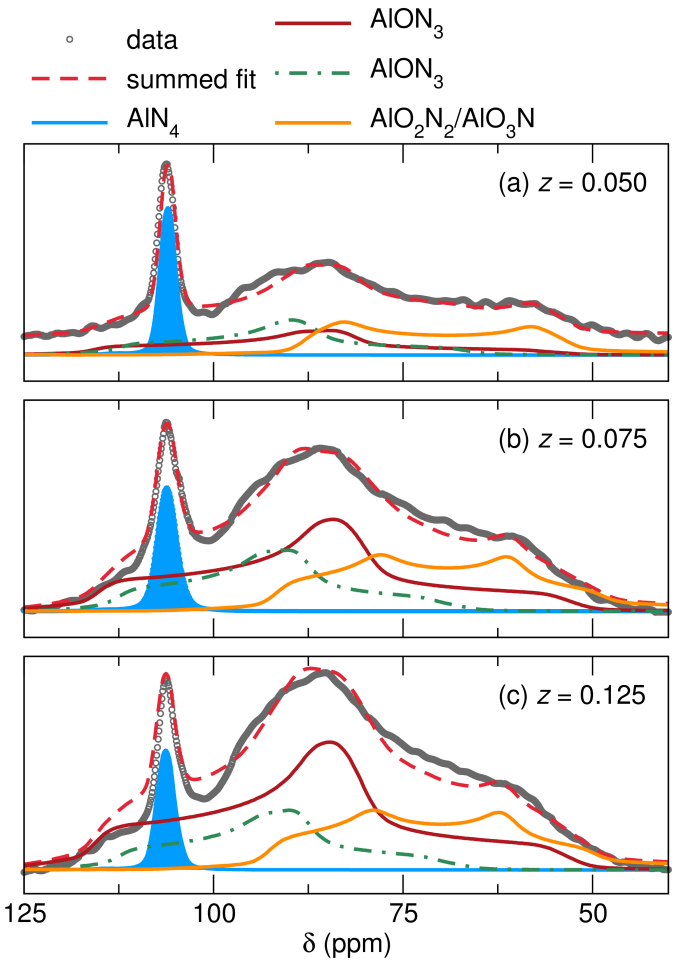

Figure 5: ^{27}Al NMR spectra at 18.8 T and 20 kHz MAS for (a) $z = 0.050$, (b) $z = 0.075$, and (c) $z = 0.125$ demonstrate the increase in the contribution from $AlON_3$ as a function of increasing Al. The experimental data (gray circles) are overlaid by the summed fit (red dashed line), which is comprised of an AlN_4 defect (blue line), two different $AlON_3$ environments (maroon and light green line), and AlO_2N_2/AlO_3N (orange line). Fit contributions are separated from data for clarity in (a).

ties of quadrupolar nuclei, would complicate inclusion of the spinning sideband manifold. Pseudo-Voigt broadening was applied. As the calculations indicate, the NMR parameters are dominated by nearest neighbors but are still significantly affected by next-nearest neighbors and beyond. While to the first coordination shell (one bond, 2.25 Å) there are only five possible local environments for Al (*i.e.,* AlO_qN_{4-q} where $0 \leq q \leq 4$), the number of distinct environments increases rapidly with cluster size. For simplicity, the smallest number of possible sites was used to achieve a satisfactory fit, but it is likely that there are many similar Al sites. C_Q values of 0 were not observed computationally or experimentally for AlO_4 or AlN_4 sites, which is due to the fact that the tetrahedra are distorted, even in the Si_3N_4 structure with no site disorder (via DFT, the EFG tensor is non-zero at the Si nucleus in Si_3N_4, but Si is an I=1/2 nucleus, meaning that cannot be observed experimentally). While the other environments could be axially symmetric with an η value close to 1, this is also not observed. The symmetry is further broken by the presence of long-range defects away from the AlO_4 or AlN_4 sites. In addition, simulations of quadrupolar NMR lineshapes for different fields and spinning rates (Supporting Information) highlight the requirement for ultrahigh field and high spinning speeds to resolve Al sites in SiAlONs. These data should prove useful for planning and executing future NMR studies of this large family of materials.

Further evidence for the experimentally observed preference for $AlON_3$ formation and its subsequent effects on the population of other tetrahedral environments is observed by comparing the experiment to a statistical model, and is shown in Figure 6. From the DFT-informed fits of the experimental NMR data, the ratio of AlN_4:$AlON_3$:AlO_2N_2/AlO_3N is 16:54:30 for $z = 0.050$, 8:64:28 for $z = 0.075$, and 7:69:24 for $z = 0.125$, with an approximate error estimate of 5% due to site overlap. The relative intensities were fit by least squares refinement with the DFT-calculated values used as initial values. A stochastic model (*i.e.*, random, statistical distribution) predicts 97.5%, 96.3%, and 93.9% AlN_4 for samples $z = 0.050$, $z = 0.075$, and $z = 0.125$, respectively, providing further evidence

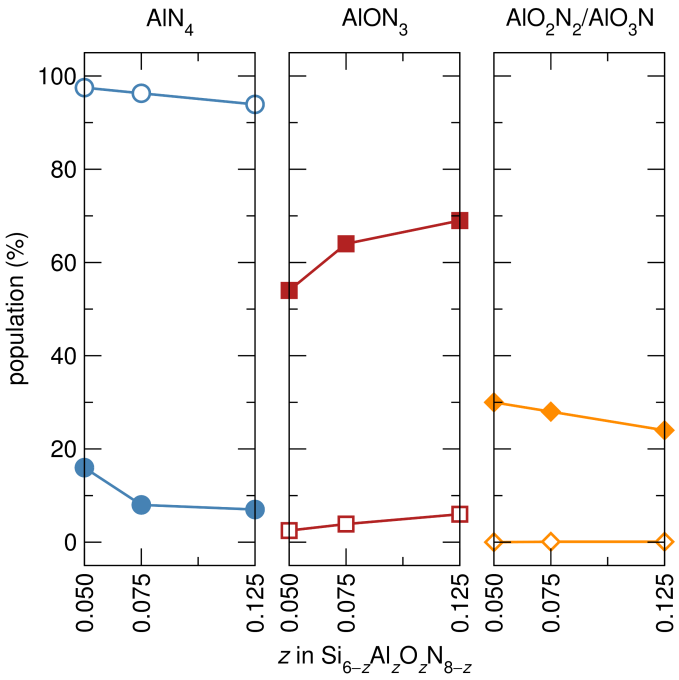

Figure 6: Populations obtained from fitting the experimental NMR data (closed shapes) show a definite preference for $AlON_3$ formation and a decrease in AlN_4 and AlO_2N_2/AlO_3N populations. This is in stark contrast to the stochastic model (open shapes), which predicts high population of AlN_4 environments, low population of $AlON_3$ tetrahedra, and virtually no AlO_2N_2/AlO_3N.

for preferential Al–O bond formation instead of a random distribution of Al and O within the Si_3N_4 structure. For $AlON_3$, the stochastic model predicts 2.5%, 3.6%, and 6.0% for $z = 0.050$, $z = 0.075$, and $z = 0.125$, respectively, and virtually zero (0.0%, 0.1%, and 0.1%) for AlO_2N_2. Thus, there is a definite preference for $AlON_3$ formation experimentally.

Table 3: Table of energy values for defects show energetic preference for $AlON_3$ bonding in two doping levels closest to that investigated experimentally. A defect is defined as the introduction of one Al–O pair.

Composition	Defect geometry (O on N1 or N2)	eV/defect
1Al-1O	AlN_4	0.00
1Al-1O	$AlON_3$ (N1)	-1.2
1Al-1O	$AlON_3$ (N2)	-1.4
2Al-2O	AlN_4	0.00
	AlN_4	
2Al-2O	AlO_2N_2 (N1, N2)	-1.1
	AlN_4	
2Al-2O	$AlON_3$ (N1)	-1.2
	$AlON_3$ (N1)	
2Al-2O	$AlON_3$ (N2)	-1.4
	$AlON_3$ (N1)	
2Al-2O	AlO_2N_2 (N1, N2)	-1.6
	$AlON_3$ (N2)	

DFT calculations of the energies for various tetrahedral environments (Figure 3) performed on a $2 \times 2 \times 2$ supercell with relaxed atomic coordinates and $z = 0.075$ lattice parameters are provided in Table 3 referenced to the least favorable configuration. Variation of the lattice parameters in the range determined from synchrotron diffraction yielded defect enthalpies within ± 0.04 eV of the intermediate lattice parameters used for enthalpy calculations. Thus, the increase in unit cell size that accompanies increased defect concentration does not significantly affect these calculations. In all defect configurations, the energy decreased as the number of Al–O bonds increased. For each composition, the baseline energy was calculated as the relaxed energy with Al only in AlN_4 tetrahedra and the corresponding number of O as OSi_3 (Figure 3a). For a single defect pair (1Al–1O) in the $2 \times 2 \times 2$ supercell (corresponding to $z = 0.125$), the localization of Al–O forms a bond

greater than 1 eV more stable than when the defect atoms are separated. In addition, it was discovered that oxygen atoms prefer to sit on the N2 site (0.2 eV–0.3 eV preference in all mixed anion tetrahedral configurations) isolated from the large hexagonal tunnel along the c-axis. Unfortunately, the two $AlON_3$ sites cannot be differentiated based on their NMR parameters, meaning the NMR data cannot be directly related to the energetics of the distinct $AlON_3$ environments. For 2 Al and 2 O, corresponding to $z = 0.25$, two adjacent AlO_2N_2 and $AlON_3$ tetrahedra with corner sharing Al atoms and oxygen corner sharing between three tetrahedra are most energetically favorable. Defects for more than 2 Al and 2 O correspond to Al contents much higher than that studied experimentally in the present work (shown in Supporting Information), where the most energetically favorable tetrahedral configurations are marked by the presence of clustered defects and an increase in the number of corner connected oxygen atoms that are joined to two Al atoms.

Simple electrostatic bond valence arguments can be made to justify the stability of Al–O pairs the β-Si_3N_4 framework. An isolated O defect on an N site would receive three charges from neighboring Si atoms, leading it to possess a net negative charge. An isolated Al defect on an Si site would have four N neighbors, each seeking a positive charge, requiring the Al to possess a net positive charge. These charge defects would annihilate and stabilize when they are nearest neighbors.

Conclusions

We have shown that Al and O have a surprising affinity for one-another in the β-SiAlON structure, despite the high dilution of both Al and O in the framework. High-field ^{27}Al solid-state NMR spectral features have been assigned to different AlO_qN_{4-q} ($0 \leq q \leq 4$) species, employing DFT calculations to help in the assignment. These results suggest unambiguously that $AlON_3$ with $q = 1$ and AlO_2N_2 with $q = 2$ are found in far greater excess than would be suggested by a stochastic distribution of Al and O on the β-Si_3N_4 framework.

DFT calculations of defect energetics on large supercells also suggest extra stabilization associated with Al–O clustering in the unit cell, which can be anticipated by electrostatic bond valence arguments. This work also shows the exquisite details of local compositional fluctuations in crystal structure that can be unravelled by the judicious combination of high-field, high-resolution NMR experiments coupled with DFT calculations.

Acknowledgement

We thank Prof. Catherine Oertel for carefully reading this manuscript. C. C. would like to thank the National Science Foundation for a Graduate Research Fellowship under Grant No. DGE 1144085. K. J. G. would like to thank The Winston Churchill Foundation of the United States and the Herchel Smith Scholarship for funding. Use of the Advanced Photon Source, an Office of Science User Facility operated for the U.S. Department of Energy (DOE) Office of Science by Argonne National Laboratory, was supported by the U.S. DOE under Contract No. DE-AC02-06CH11357. DFT calculations were performed on the Darwin Supercomputer of the University of Cambridge High Performance Computing Service (http://www.hpc.cam.ac.uk/), provided by Dell Inc. using Strategic Research Infrastructure Funding from the Higher Education Funding Council for England and funding from the Science and Technology Facilities Council (UK). This work made use of MRL shared experimental facilities, supported by the MRSEC Program of the NSF under Award No. DMR 1121053. The MRL is a member of the NSF-funded Materials Research Facilities Network (www.mrfn.org). Data supporting this work are available from www.repository.cam.ac.uk.

Supporting Information: Reference equation for ^{27}Al shifts, model stochastic calculations, energetics for higher doping levels, calculated NMR spectra for different fields and MAS rates.

References

(1) Cao, G.; Metselaar, R. α'-Sialon ceramics: a review, *Chem. Mater.* **1991**, *3*, 242–252.

(2) Attfield, J. P. Principles and applications of anion order in solid oxynitrides, *Cryst. Growth Des.* **2013**, *13*, 4623–4629.

(3) Butler, N.; Dupree, R.; Lewis, M. H. The use of magic-angle-spinning NMR in structural studies of Si-Al-ON phases, *J. Mater. Sci. Lett.* **1984**, *3*, 469–470.

(4) Sjöberg, J.; Harris, R. K.; Apperley, D. C. ^{29}Si, ^{27}Al and ^{15}N magic-angle spinning nuclear magnetic resonance study of O'-Sialons and some related phases, *J. Mater. Chem.* **1992**, *2*, 433–438.

(5) Dupree, R.; Lewis, M.; Leng-Ward, G.; Williams, D. Co-ordination of Si atoms in silicon-oxynitrides determined by magic-angle-spinning NMR, *J. Mater. Sci. Lett.* **1985**, *4*, 393–395.

(6) Smith, M. E. Observation of mixed aluminum oxynitride (Al(O, N)$_4$) structural units by aluminum-27 magic angle spinning NMR, *J. Phys. Chem.* **1992**, *96*, 1444–1448.

(7) Vinograd, V. L.; Juarez-Arellano, E. A.; Lieb, A.; Knorr, K.; Schnick, W.; Gale, J. D.; Winkler, B. Coupled Al/Si and O/N order/disorder in BaYb[$Si_{4-x}Al_xO_xN_{7-x}$] sialon: neutron powder diffraction and Monte Carlo simulations, *Z. Kristallogr.* **2007**, *222*, 402–415.

(8) Dupree, R.; Lewis, M. H.; Smith, M. Structural characterization of ceramic phases with high-resolution ^{27}Al NMR, *J. Appl. Crystallogr.* **1988**, *21*, 109–116.

(9) Klinowski, J.; Thomas, J.; Thompson, D.; Korgul, P.; Jack, K.; Fyfe, C.; Gobbi, G. Structural studies of sialon ceramics by high-resolution solid-state NMR, *Polyhedron* **1984**, *3*, 1267–1269.

(10) Tatsumi, K.; Mizoguchi, T.; Yoshioka, S.; Yamamoto, T.; Suga, T.; Sekine, T.; Tanaka, I. Distribution of solute atoms in β-and spinel $Si_{6-z}Al_zO_zN_{8-z}$ by Al K-edge X-ray absorption near-edge structure, *Phys. Rev. B* **2005**, *71*, 033202.

(11) Brgoch, J.; Gaultois, M. W.; Balasubramanian, M.; Page, K.; Hong, B.-C.; Seshadri, R. Local structure and structural rigidity of the green phosphor β-SiAlON:Eu^{2+}, *Appl. Phys. Lett.* **2014**, *105*, 181904.

(12) Lippmaa, E.; Mägi, M.; Samoson, A.; Tarmak, M.; Engelhardt, G. Investigation of the structure of zeolites by solid-state high-resolution silicon-29 NMR spectroscopy, *J. Am. Chem. Soc.* **1981**, *103*, 4992–4996.

(13) George, N. C.; Pell, A. J.; Dantelle, G.; Page, K.; Llobet, A.; Balasubramanian, M.; Pintacuda, G.; Chmelka, B. F.; Seshadri, R. Local environments of dilute activator ions in the solid-state lighting phosphor $Y_{3-x}Ce_xAl_5O_{12}$, *Chem. Mater.* **2013**, *25*, 3979–3995.

(14) Furdyna, J. K. Diluted magnetic semiconductors, *J. Appl. Phys.* **1988**, *64*, R29–R64.

(15) Hsu, K. F.; Loo, S.; Guo, F.; Chen, W.; Dyck, J. S.; Uher, C.; Hogan, T.; Polychroniadis, E.; Kanatzidis, M. G. Cubic $AgPb_mSbTe_{2+m}$: bulk thermoelectric materials with high figure of merit, *Science* **2004**, *303*, 818–821.

(16) Larson, A. C.; Von Dreele, R. B. GSAS, *General Structure Analysis System. LANSCE, MS-H805, Los Alamos, New Mexico* **1994**,

(17) Toby, B. H. EXPGUI, a graphical user interface for GSAS, *J. Appl. Crystallogr.* **2001**, *34*, 210–213.

(18) Momma, K.; Izumi, F. VESTA: a three-dimensional visualization system for electronic and structural analysis, *J. Appl. Crystallogr.* **2008**, *41*, 653–658.

(19) Clark, S. J.; Segall, M. D.; Pickard, C. J.; Hasnip, P. J.; Probert, M. I.; Refson, K.;

Payne, M. C. First principles methods using CASTEP, *Z. Kristallogr.* **2005**, *220*, 567–570.

(20) Pickard, C. J.; Mauri, F. All-electron magnetic response with pseudopotentials: NMR chemical shifts, *Phys. Rev. B* **2001**, *63*, 245101.

(21) Yates, J. R.; Pickard, C. J.; Mauri, F. Calculation of NMR chemical shifts for extended systems using ultrasoft pseudopotentials, *Phys. Rev. B* **2007**, *76*, 024401.

(22) Profeta, M.; Mauri, F.; Pickard, C. J. Accurate first principles prediction of ^{17}O NMR parameters in SiO_2: assignment of the zeolite ferrierite spectrum, *J. Am. Chem. Soc.* **2003**, *125*, 541–548.

(23) Perdew, J. P.; Burke, K.; Ernzerhof, M. Generalized gradient approximation made simple, *Phys. Rev. Lett.* **1996**, *77*, 3865.

(24) Monkhorst, H. J.; Pack, J. D. Special points for Brillouin-zone integrations, *Phys. Rev. B* **1976**, *13*, 5188.

(25) Bak, M.; Rasmussen, J. T.; Nielsen, N. C. SIMPSON: a general simulation program for solid-state NMR spectroscopy, *J. Magn. Reson.* **2000**, *147*, 296–330.

(26) Zhu, X.; Masubuchi, Y.; Motohashi, T.; Kikkawa, S. The z value dependence of photoluminescence in Eu^{2+}-doped β-SiAlON ($Si_{6-z}Al_zO_zN_{8-z}$) with $1 \leq z \leq 4$, *J. Alloys Compd.* **2010**, *489*, 157–161.

(27) Takeda, T.; Xie, R.-J.; Hirosaki, N. Local structure analysis in nitride and oxynitride phosphors, *ECS J. Solid State Sci. Technol.* **2013**, *2*, R3132–R3137.

(28) Denault, K. A.; Brgoch, J.; Kloß, S. D.; Gaultois, M. W.; Siewenie, J.; Page, K.; Seshadri, R. Average and Local structure, Debye temperature, and structural rigidity in some oxide compounds related to phosphor hosts, *ACS Appl. Mater. Interfaces* **2015**, *7*, 7264–7272.

(29) Shannon, R. Effective ionic radii in oxides and fluorides, *Acta Crystallogr. B.* **1969**, *25*, 925–46.

For Table of Contents Only

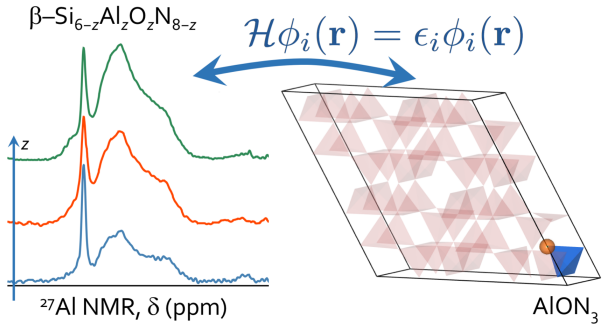

High-field ^{27}Al solid-state nuclear magnetic resonance (NMR) studies, coupled with density functional theory calculations of NMR parameters and energetics, suggest that even in samples of the β-SiAlON β-$Si_{6-z}Al_zO_zN_{8-z}$ with small values of z, that Al and O tend to cluster, with a high propensity for $AlON_3$ tetrahedral motifs to be distributed on the SiAlON framework.

Supporting information for Structural evolution and atom clustering in β-SiAlON: β-$Si_{6-z}Al_zO_zN_{8-z}$

Clayton Cozzan,[†,‡,¶] Kent J. Griffith,[§] Geneva Laurita,[†,¶]

Jerry G. Hu,[¶] Clare P. Grey,[*,§] and Ram Seshadri[*†,‡,¶,//]

†*Mitsubishi Chemical Center for Advanced Materials, University of California Santa Barbara, California 93106, United States*

‡*Materials Department, University of California Santa Barbara, California 93106, United States*

¶*Materials Research Laboratory, University of California Santa Barbara, California 93106, United States*

§*Department of Chemistry, University of Cambridge Lensfield Road, Cambridge CB2 1EW, United Kingdom*

// *Department of Chemistry and Biochemistry, University of California Santa Barbara, California 93106, United States*

E-mail: cpg27@cam.ac.uk; seshadri@mrl.ucsb.edu

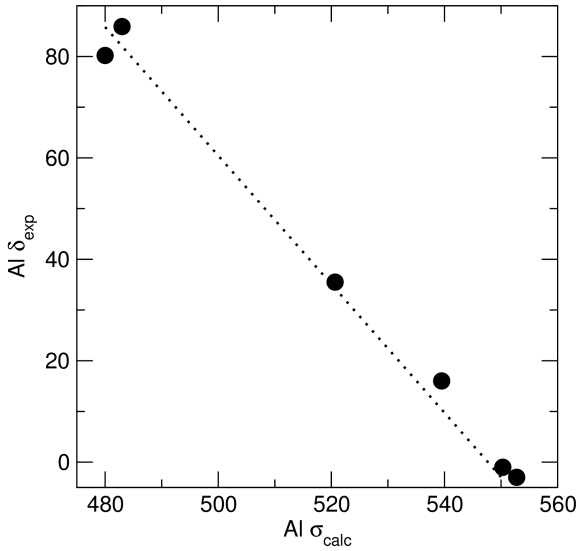

Figure S1: Plot of calculated ^{27}Al shielding versus chemical shift for reference compounds Al_2O_3 (corundum), $Ca_{12}Al_{14}O_{33}$, $Na_5Al_3F_{14}$, and Al_2SiO_5 (andalusite). Linear regression yielded the expression $\delta_{exp}(^{27}Al) = -1.20\sigma_{calc}(^{27}Al) + 661$ with an R^2 value of 0.9932, indicating a small degree of scatter in the points. NMR shifts are conventionally referenced to an arbitrary compound. In the case of ^{27}Al, 1 M $Al(NO_3)_{3\ (aq.)}$ is defined as 0.0 ppm. Quantum calculations provide a value for chemical shielding, which can be converted to shift through the use of (a) reference compound(s). Note that any error in the conversion from shielding to shift will affect all compounds in the study uniformly such that relative shift relationships are more reliable than absolute shifts.

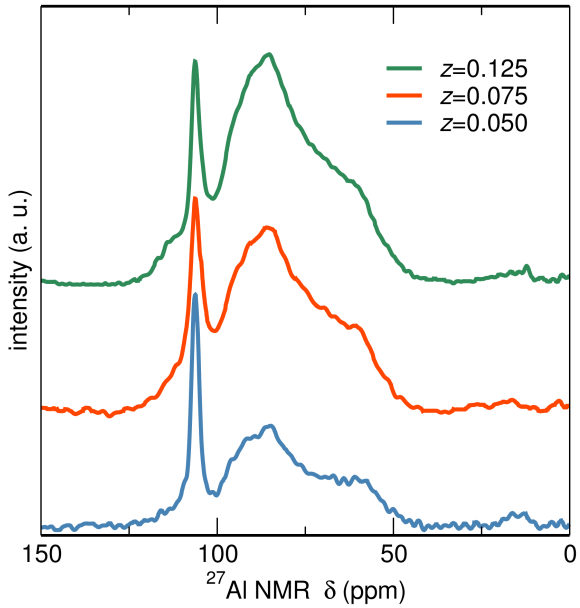

Figure S2: Raw ^{27}Al NMR data for z=0.125 (green), z=0.075 (red), and z=0.050 (blue) in β-$Si_{6-z}Al_zO_zN_{8-z}$.

The mathematical explanation behind the stochastic model is described below. The number of configurations (*n.o.c.*) of a given coordination type α e.g., $AlON_3$ is as follows (Eqn. 1):

$$n.o.c._{\alpha} = \frac{(a+b)!}{(a!)(b!)} \quad (1)$$

where a is the number of species A in the coordination shell e.g., 1 O, and b is the number of species B in the coordination shell e.g., 3 N. Using $n.o.c._{\alpha}$, the probability of that given coordination type (p_{α}) can be calculated as follows (Eqn. 2):

$$p_{\alpha} = n.o.c._{\alpha}\,([A]^{a} \times [B]^{b}) \quad (2)$$

where $[A]$ is the concentration of species A e.g., 0.05/8 = 0.00625 and $[B]$ is the concentration of species B e.g., 7.95/8 = 0.99375. The total probability of all sites (Eqn. 3) and the sum of all concentrations (Eqn. 4) must each equal unity.

$$p_{total} = p_{\alpha} + p_{\beta} + p_{\ldots} = 1 \quad (3)$$

$$[A] + [B] + [\ldots] = 1 \quad (4)$$

The results of the stochastic model for the current work, a tetrahedral ion with two coordination species, are detailed below in Table S1, with $p_{0.050}$, $p_{0.075}$, and $p_{0.125}$ corresponding to the experimentally observed doping concentrations, z = 0.050, z = 0.075, and z = 0.125, respectively.

Table S1. Stochastic coordination model for a tetrahedral ion with two coordinating species. The statistical probability for each AlO_yN_{4-y} site is calculated for various dopant concentrations in $Si_{6-z}Al_zO_zN_{8-z}$. At the defect concentrations in this study, z = 0.05, z = 0.075, and z = 0.125, a random distribution of atoms would yield AlN_4 tetrahedra with a minor presence of $AlON_3$.

Config.	O	N	*n.o.c.*	$p_{0.050}$ (%)	$p_{0.075}$ (%)	$p_{0.125}$ (%)	$p_{0.50}$ (%)	$p_{1.00}$ (%)	$p_{2.00}$ (%)	$p_{4.00}$ (%)
AlN_4	0	4	1	97.5	96.3	93.9	77.2	58.6	31.6	6.3
$AlON_3$	1	3	4	2.5	3.6	6.0	20.6	33.5	42.2	25.0
AlO_2N_2	2	2	6	0.0	0.1	0.1	2.1	7.2	21.1	37.5
AlO_3N	3	1	4	0.0	0.0	0.0	0.1	0.7	4.7	25.0
AlO_4	4	0	1	0.0	0.0	0.0	0.0	0.0	0.4	6.3

Table S2: Defect energies corresponding to Al contents greater than those investigated experimentally. Energy preference is normalized by the least favorable configuration, i.e. isolated AlN_4 and OSi_3. In addition to statistical probabilities, energetics for specific dopant amounts were also explored. Table S2 provides energy values for defects greater than that measured experimentally, which continue to show energetic preference for defect Al–O clustering.

Composition	Site (O on N1 or N2)	Energy/enthalpy (eV)	Energy preference (eV/formula unit)
3Al-3O	AlN_4 AlN_4 AlN_4	-26313.26	0
3Al-3O (adjacent tetrahedra)	$AlON_3$ (N1) $AlON_3$ (N2) $AlON_3$ (N1)	-26315.87	-2.61
3Al-3O (isolated tetrahedra)	$AlON_3$ (N1) $AlON_3$ (N2) $AlON_3$ (N1)	-26316.06	-2.80
3Al-3O	AlO_3N (N1, N1, N2) AlN_4 $AlON_3$ (N2)	-26315.98	-2.72
3Al-3O (adjacent tetrahedra)	AlO_3N (N1, N1, N2) AlN_4 AlN_4	-26315.08	-1.82
3Al-3O (isolated tetrahedra)	AlO_3N (N1, N1, N1) AlN_4 AlN_4	-26314.76	-1.50
4Al-4O	AlN_4 AlN_4 AlN_4 AlN_4	-26415.56	0
4Al-4O	AlO_2N_2 (N1, N1) $AlON_3$ (N2) AlO_2N_2 (N1, N1) $AlON_3$ (N1)	-26420.38	-4.81
4Al-4O	$AlON_3$ (N2) AlN_4 AlO_2N_2 (N1, N1) $AlON_3$ (N1)	-26418.88	-3.31
4Al-4O	AlN_4 AlO4 (N1, N1, N1, N2) $AlON_3$ (N1) AlN_4	-26419.11	-3.55

4Al-4O	$AlON_3$ (N1) AlN_4 AlO_3N (N1, N1, N2) $AlON_3$ (N1)	-26419.9	-4.34
4Al-4O	$AlON_3$ (N1) AlN_4 AlO_3N (N1, N1, N1) AlO_2N_2 (N1, N1)	-26420.23	-4.66

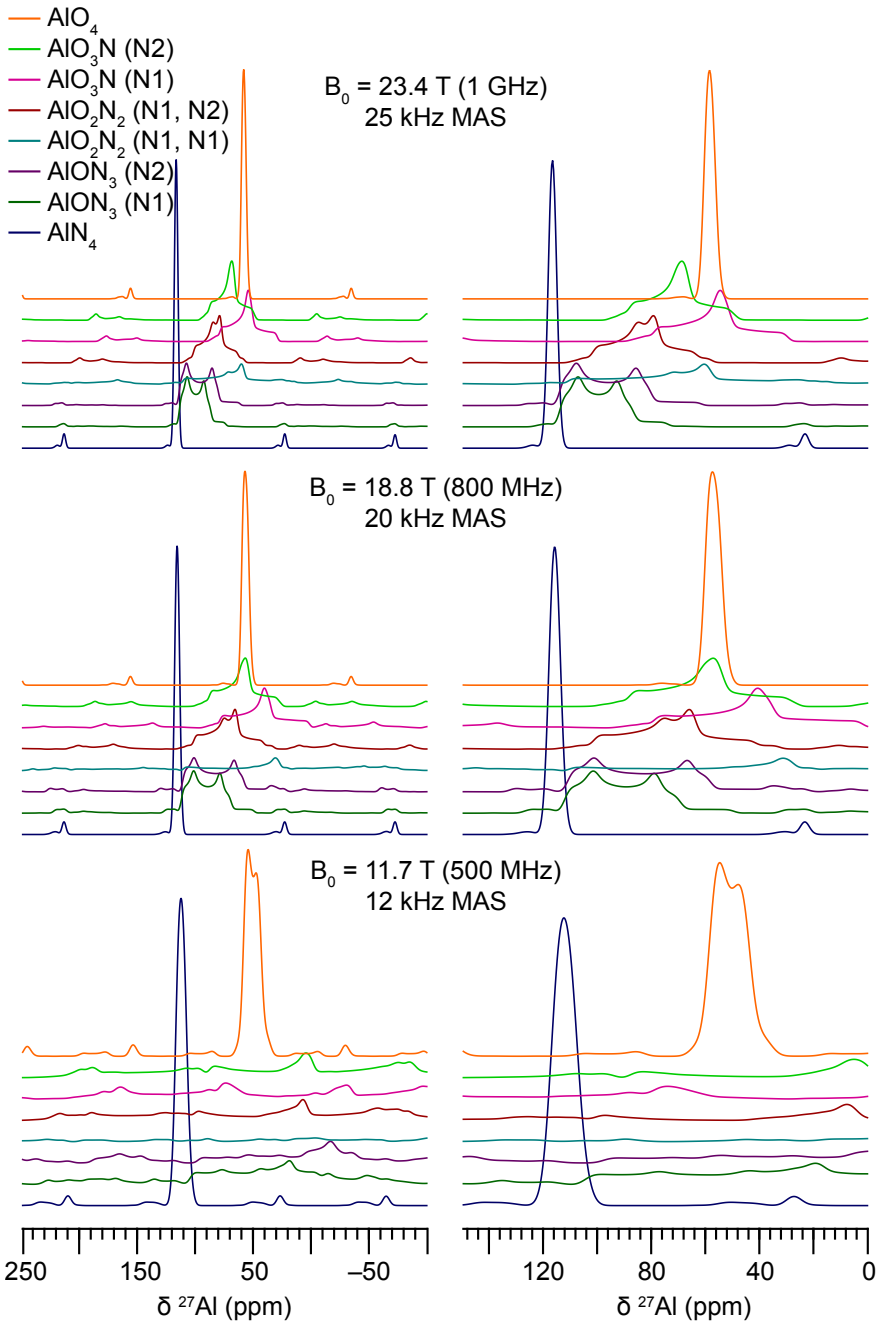

Figure S3: Calculated ^{27}Al MAS NMR spectra for the possible coordination environments of aluminum in SiAlON at different magnetic fields and MAS rates showing that the strongly quadrupolar ^{27}Al environments of mixed anion $Al(O,N)_4$ tetrahedra can only be resolved—or even observed—in ultrahigh magnetic fields. N1 and N2 designates where the oxygen atom(s) is(are) located between the crystallographically distinct anion sites. Each cation coordinates to three N1 sites and one N2 site; thus, the undesignated sites in AlO_3N and AlO_4 can be inferred.